ACS APPLIED MATERIALS & INTERFACES

RESEARCH ARTICLE

www.acsami.org

Er-Doped ZnO Nanorod Arrays with Enhanced 1540 nm Emission By Employing Ag Island Films and High-Temperature Annealing

Jian-Wei Lo,[†,§] Wei-Cheng Lien,[†,‡] Chin-An Lin,[†,§] and Jr-Hau He[*,†,§]

[†]Institute of Photonics and Optoelectronics and [§]Department of Electrical Engineering, National Taiwan University, Taipei, 10617 Taiwan

[‡]Berkeley Sensor and Actuator Center, University of California, Berkeley, California, United States

ABSTRACT: Single-crystalline Er-doped ZnO nanorod arrays (NRAs) on Ag island films with appropriate annealing show a promising enhancement of 1540 nm emission for optical communication. The enhanced 1540 nm emission of Er-doped ZnO NRAs is attributed to the enhancement of the deep level emission of ZnO host. In an effort to enhance deep level emission to pump Er^{3+} emission at 1540 nm in the Er-doped ZnO NRAs, surface plasmon coupling and increase in deep level states were carried out via Ag island films and high-temperature annealing. This study points to the effective methods to enhance 1540 nm emission, demonstrating that ZnO NRAs with Ag islands have a promising potential for the application in optical communications.

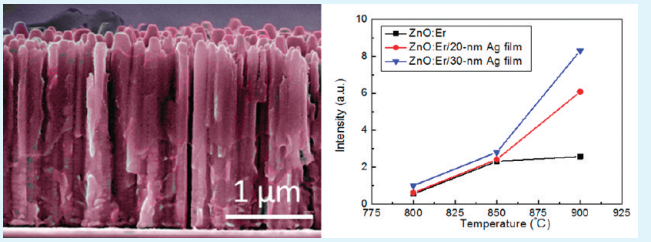

KEYWORDS: ZnO, nanorod, nanowire, Er^{+3} emission

INTRODUCTION

Erbium (Er)-doped semiconductors have drawn considerable attentions over the decades, because the transition of Er intra-4f shell can cause an emission at 1540 nm, which locates in the region of optical communication with minimum loss.[1,2] It has been reported that the Er-related emission of 1540 nm can be enhanced by annealing,[3] oxygen doping,[4] and the use of wide bandgap materials.[5−8] Regarding the incorporation of Er in ZnO nanorods, it has been reported that the emission from Er^{3+} ions is very sensitive to the local site symmetry of Er ions, which has been verified by the spectroscopic investigation.[9−12]

ZnO is a promising candidate as a host material for Er doping because it is possessed with the wide bandgap of 3.3 eV at room temperature and oxygen is one of major elements in ZnO. Er-doped ZnO films have been proved as reliable materials for light-emitting diodes, laser diodes, optical amplifiers at 1540 nm in the waveguide structures as well as electrode materials for carrier injection because of their high electrical conductivities.[13] However, the relatively low solubility of Er atoms in ZnO leads to low luminescent efficiency of the Er-related emission.[14] The nanostructured materials are thus designed to increase the solubility by increasing the surface area of material.[4,15−18] Recently, successful optical activations of ZnO nanowires by Er ion implantation and chemical methods have been reported,[4,15,16] demonstrating the potential of the one-dimensional ZnO as a new material platform for optical communication.

Furthermore, native defects are the major contributions of the n-type semiconducting behavior of ZnO and related to the deep level emission, which causes the visible luminescence.[19−21] It has been reported that the electron excitation from ground state ($^4I_{15/2}$) to 4f levels pumped by deep level-mediated excitation dominates Er^{3+} emission, as compared with that excited by bandgap-absorbed light; i.e., the energy transfer from the electron-hole recombination at deep level states provides an efficient excitation route for Er^{3+} emission.[22] This is due to the fact that the energy (526 nm) for the transition between the $^2H_{11/2}$ state and the ground $^4I_{15/2}$ state of Er^{3+} is close to the energy of the deep level emission, opening more possibilities of energy transfer towards Er^{3+} via the resonant coupling.

Recently, the surface plasmon has been found to enhance the luminescent efficiency with the merit of easily tuning the resonance band by various metal island coatings,[23] allowing the field enhancement in wide energy ranges. For example, Okamoto et al. have reported that the photoluminescence (PL) intensity of InGaN quantum wells is enhanced by coating Ag island layers.[24] Cheng et al. have found that the emissions in ZnO thin films could be significantly enhanced via surface plasmon coupling with Ag island films.[25] The coupling of emission energy to surface plasmon energy, which is controlled by the size of the metal island films, has been demonstrated to be decisive for light emission enhancement.[26]

In this study, we employed the surface plasmon effect and increased deep level states to enhance the deep level emission, leading to the enhancement of Er^{3+} emission at 1540 nm in the single-crystal Er-doped ZnO nanorod arrays (NRAs). Coupling the surface plasmon to the deep level emission was achieved by the introduction of Ag island films. High-temperature annealing was utilized to increase the density of deep level states. This study demonstrates that Er-doped ZnO NRAs are potentially a viable

Received: October 25, 2010
Accepted: March 15, 2011
Published: April 01, 2011

ACS Publications © 2011 American Chemical Society

dx.doi.org/10.1021/am101031f | *ACS Appl. Mater. Interfaces* 2011, 3, 1009–1014

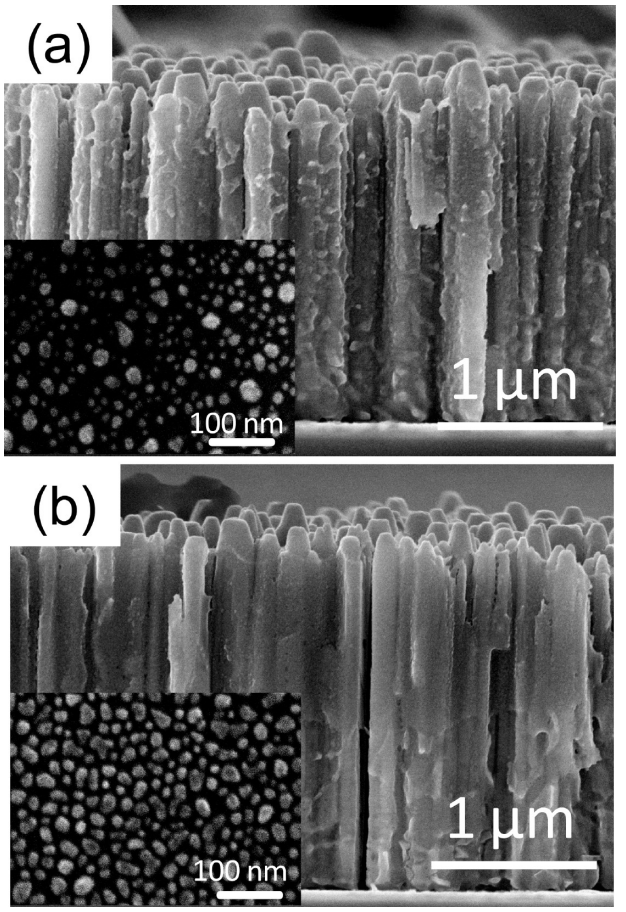

Figure 1. Cross-sectional SEM image of Er-doped ZnO NRAs grown on (a) 20 and (b) 30 nm thick Ag island films. The insets of a and b are the surface morphologies of 20 and 30 nm thick Ag island films on Si substrates, respectively.

candidate for optoelectronic devices operating in the 1540 nm region.

EXPERIMENTAL SECTION

Si(100) wafers with a resistivity of 2 Ω cm were used as substrates. The Si(100) substrates were first coated with 20 and 30 nm thick Ag island films by the ULVAC CRTM-6000 e-gun evaporator equipped with a quartz crystal thickness monitor. The ZnO NRAs were grown on Si(100) substrates using the hydrothermal process.[27] Briefly, a thin zinc acetate film was spin-coated on the bare Si substrate and Ag islands/Si with an ethanol solution containing 5 mM zinc acetate dihydrate. After annealing at 300 °C for 30 minutes in air ambient, ZnO seed layers with the thickness of 5-10 nm were then yielded. ZnO NRAs were grown on ZnO seed layers in ammonia aqueous solution containing 10 nM zinc nitrate hexahydrate at 95 °C for 2 h. The reactants were then cooled to room temperature and the substrate was rinsed with ethanol to remove the impurities. After drying with the nitrogen gas, the as-grown ZnO NRAs were then spin-coated with approximately 3.5 nm thick erbium chloride hexahydrate in ethanol solution. The as-coated samples were then annealed at 800, 850, and 900 °C in the furnace for 4 h in air ambient.

The microstructure was characterized with grazing incidence X-ray diffractometry (XRD) with the X-ray source of a Cu K_α line and a JEOL 2100 transmission electron microscope (TEM) operating at 200 kV. Morphological studies of the synthesized nanostructures were performed with a JEOL JSM-6500 field-emission scanning electron microscope (SEM). The electronic structures of NRAs were confirmed by PHI Quantera x-ray photoelectron spectroscope (XPS). The 325 nm He−Cd laser was used for UV/visible and IR PL measurements. The absorption spectra were measured with a JASCO V-670 UV−visible spectrometer.

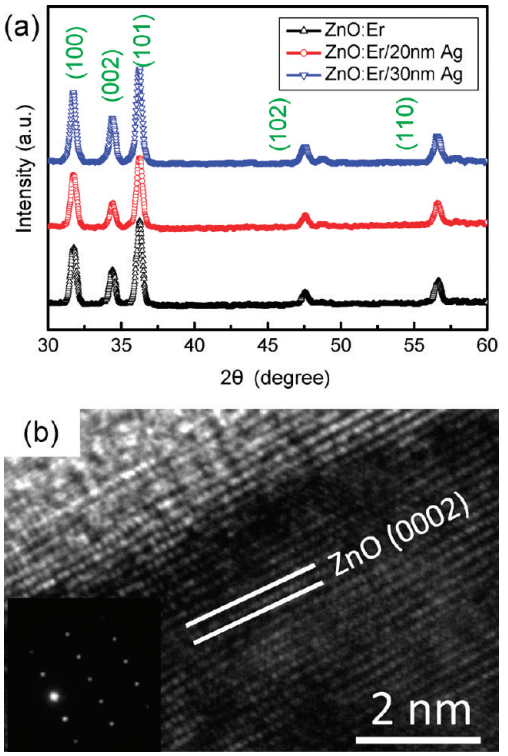

Figure 2. (a) XRD spectra of Er-doped ZnO NRAs grown on bare Si substrates, 20 and 30 nm thick Ag island films. (b) HRTEM image of an Er-doped ZnO nanorod. The inset in b shows the corresponding selected-area electron diffraction pattern. The intensity is shifted on purpose as a guide to the eye for distinguishing every spectrum in a.

RESULTS AND DISCUSSION

In order to investigate the influences of the surface plasmon on the enhancement of the light emitting efficiency, different thicknesses of Ag island films are deposited on Si(100) substrates. The insets of Figure 1a,b show the surface morphologies of 20 and 30 nm thick Ag island films, respectively. The grain size of Ag islands increases as the film thickness increases monitored by a thickness monitor. After coating with the ZnO seed layers, hydrothermal growth and subsequent Er-doping process, Er-doped ZnO NRAs grown on Ag island films are obtained, as shown in Figure 1. The ZnO NRAs exhibit the similar diameter of 200 ± 20 nm and the length of approximately 2 μm for different Ag island films, which suggests that the underneath Ag coatings do not affect the growth of the ZnO NRAs.

The microstructures of Er-doped ZnO NRAs on Ag island films are investigated by XRD and TEM. Figure 2a shows the XRD spectra of the Er-doped ZnO NRAs grown on Si substrates with the different thicknesses of Ag island films. For all three cases, all the diffraction peaks can be indexed to the wurtzite ZnO structure and there is no new phase, such as Er_2O_3, formed after Er-doping in ZnO NRAs, indicating that Er atoms are incorporated within ZnO NRAs successfully.[16] An HRTEM image and the corresponding selected-area electron diffraction pattern of an

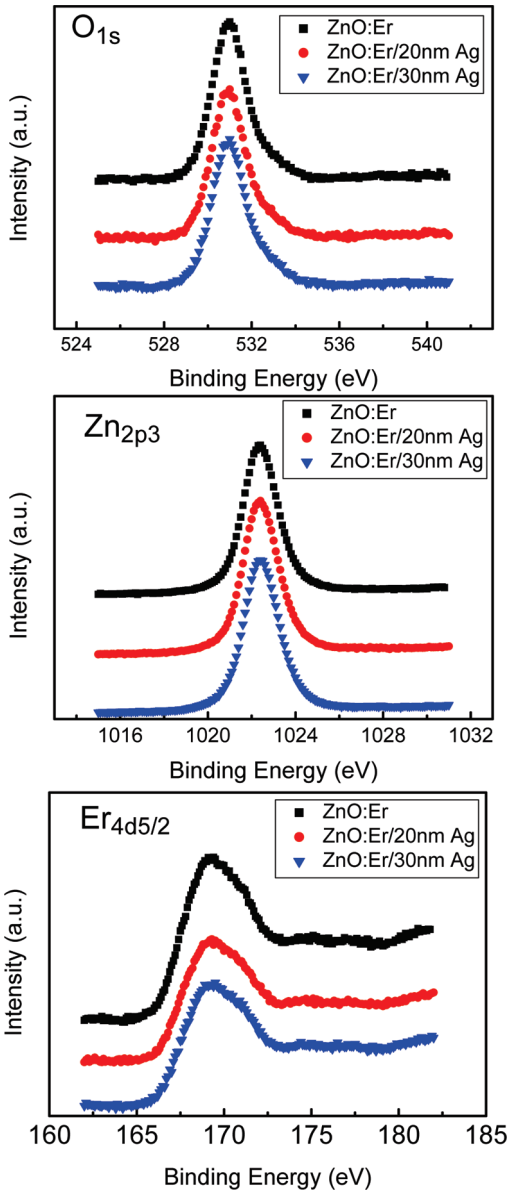

Figure 3. XPS spectra of O_{1s}, $Zn_{2p3/2}$, and $Er_{4d5/2}$ core levels of Er-doped ZnO NRAs on the Si substrates with different thicknesses of Ag island films annealed at 800 °C. The intensity is shifted on purpose as a guide to the eye for distinguishing every spectrum.

Er-doped ZnO nanorod are shown in Figure 2b, confirming that the Er-doped ZnO nanorod exhibits a wurtzite structure and the growth direction is along [0001] direction. The interplanar spacing of approximately 0.26 nm measured from the fringe pattern of the HRTEM image corresponds to the (0002) lattice spacing of ZnO.[28]

The electronic structures and chemical compositions of Er-doped ZnO NRAs are examined using XPS measurements. The surfaces of all samples are cleaned by Ar^+ ion etching prior to the XPS measurements. A chemical shift of the binding energy (BE) is calibrated by C_{1s} signal from the adsorbed surface at 285.0 eV. Figure 3 shows the XPS spectra with the binding states of the three compositional elements, namely O_{1s}, $Zn_{2p3/2}$, and $Er_{4d5/2}$ core levels in the Er-doped ZnO NRAs grown on the Si substrates with different thicknesses of Ag island films. The O_{1s} signal presents a line shape at BE= 531 eV. The BE of the $Zn_{2p3/2}$ is close to 1022.4 eV, referring to the zinc(II) oxide.[29] The Er_{4d} signal presents a complex shape, related to the coupling phenomena between the 4d hole and the lanthanide partially filled 4f shell. In particular, negligible variations in the position and the shape of the most intense 4d5/2 spin-orbit split component at 169.3 eV indicate the same electronic structures of Er(III) species in ZnO with different thicknesses of Ag island films.[29,30] Because the number of photoelectrons of an element depends on the atomic concentration, XPS measurements are useful to quantify the chemical compositions. It is found that the compositions of Zn, O and Er are independent with the thickness of Ag island films because the ratio of these integrated intensities is almost identical for these three samples, suggesting that the light emission efficiency is not be affected by the chemical compositions of Zn, O, and Er.

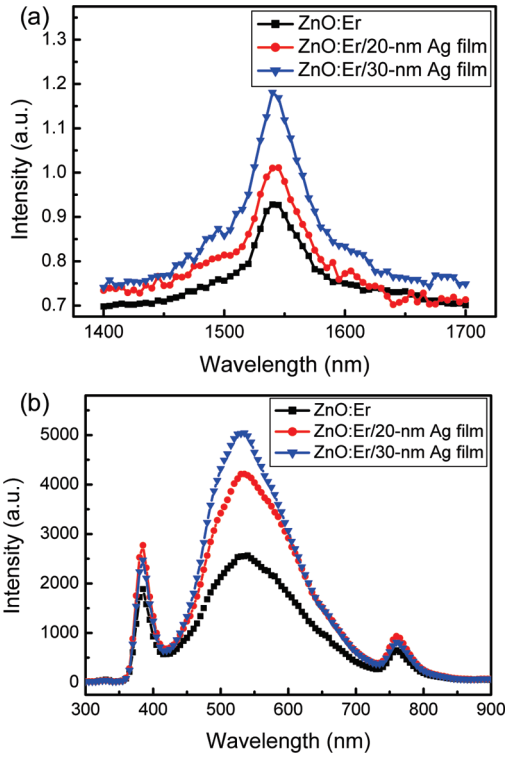

Figure 4. (a) IR PL spectra and (b) UV/visible spectra of Er-doped ZnO NRAs on the bare Si and Ag/Si substrates with the various thicknesses of the Ag films.

Figure 4a shows the IR PL spectra of Er-doped ZnO NRAs on bare Si, 20 and 30 nm thick Ag island films/Si substrates under a 325 nm He−Cd laser excitation. The PL peak intensity of 1540 nm, corresponding to the intra-4f shell transition of Er^{3+} ions, increases with the thickness of Ag island films. This Er-related emission is considered to be induced by the 325 nm laser to generate the electron-hole pairs of ZnO NRAs, and the absorbed energy of ZnO NRAs is then transferred to excite the Er^{3+} to the different excited states. Afterward, the part of excited Er^{3+} ions is released from the first excited state ($^4I_{13/2}$) to the ground state ($^4I_{15/2}$) to generate the light emission at 1540 nm. This 1540 nm emission also indicates that the Er atoms are successfully doped into the ZnO lattice by the proposed simple wet chemical reaction and the subsequent annealing process. The unchanged shapes of the IR PL spectra for all samples

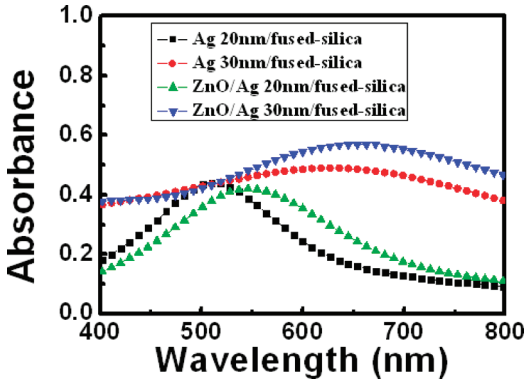

Figure 5. Absorption spectra of 20 and 30 nm thick Ag island films/fused silica substrates, and the 5 nm thick ZnO seed layer on 20 and 30 nm thick Ag island films/fused silica after annealed at 300 °C in air for 25 min.

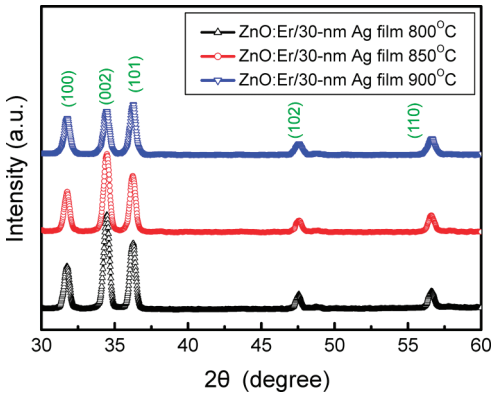

Figure 6. XRD spectra of Er-doped ZnO NRAs grown on 30 nm thick Ag/Si substrates with the annealing temperatures of 800, 850, and 900 °C. The intensity is shifted on purpose as a guide to the eye for distinguishing every spectrum.

indicate that the Er-doped ZnO NRAs grown on the different thicknesses Ag island films/Si substrates exhibit the same placement of Zn and O atoms around Er atoms since the spectrum shape of 1540 nm concerns the local structure around Er atoms.[31]

The UV/visible PL measurements have been performed to further confirm the origin of the enhanced 1540 nm PL intensity as the thickness of Ag island films increases. Figure 4b is the UV/visible PL spectra of Er-doped ZnO NRAs on bare Si and different thicknesses of Ag island films on Si. The peaks located at 382 nm and 540 nm represent a near-band-edge emission and a deep level emission, respectively.[16,32] The deep level emission at 540 nm increases with the thickness of Ag island films. The peak intensity of the deep level emission at 540 nm is strongly related to the density of the native defects, such as O vacancies.[33] On the basis of the XPS analysis, the identical shapes of O_{1s} indicates that the densities of O defects in Er-doped ZnO NRAs grown on different thicknesses of Ag island films are similar. Therefore, the deteriorated crystallinity of ZnO NRAs is not observed after the introduction of Ag island films and thus is not responsible for the enhanced 540 nm emission. It has been reported that the enhancement of deep level emission at 540 nm of ZnO host can be achieved via coupling with surface plasmon of metals, such as Ag.[25] To characterize the excited surface plasmon resonance modes, the UV−visible absorption spectra of 20 and 30 nm thick Ag island films/fused silica substrates with and without 5 nm thick ZnO seed layers are shown in Fig. 5. Since the Si substrate has a high refractive index and a high absorption coefficient which hinders the extraction of the information in the extinction spectrum. The fused silica is used as the substrate instead of the Si. The energy of the surface plasmon resonance strongly depends on the dielectric constant of thin dielectric layers, the size, and the shape of these metal islands.[25,34−37] It can be seen that the large Ag islands lead to the increasing intensity of the absorption with the redshift.[25,38] The broad absorption spectra are attributed to the irregular size of the Ag islands. By taking into account the different dielectric constants of ZnO and air, the different resonance frequencies between ZnO/Ag and air/Ag are obtained as shown in Fig. 5. In a word, Ag islands could serve as a radiative antenna to enhance the deep level emission of Er-doped ZnO NRAs at 540 nm via coupling surface plasmon. In addition, the difference of the enhanced ratio of visible emission (~540 nm) to UV emission (~380 nm) excludes the possibility of the enhanced 540 nm emission of Er-doped ZnO NRAs by the metal reflection.

It is thought that the 540 nm excitations directly pumping the Er^{3+} ions from the ground states of $^4I_{15/2}$ to the excited states of $^2H_{11/2}$ leads to more efficient 1540 nm emission due to energy coupling, as compared with the excitation of ZnO host via near-band-edge absorption.[13] A detailed mechanism of the enhanced 1540 nm PL intensity of Er-doped ZnO NRAs is proposed as follows. Initially, a pumping source of the 325 nm He−Cd laser generates the electron-hole pairs of the Er-doped ZnO NRAs, and the deep level states existing in the band gap of ZnO host could serve as the effective energy transfer media for the Er^{3+} ion excitation.[13,15] This is because that 2.63 eV (526 nm), corresponding to the energy transition between the $^2H_{11/2}$ state and the ground $^4I_{15/2}$ state of Er^{3+}, lies inside the enhanced deep level emission coupling with surface plasmon of Ag islands, opening more possibilities of energy transfer towards Er^{3+} due to resonance coupling. The Er ions in the ground states resonantly absorb more energy related to the deep levels of ZnO host (540 nm) and are excited from the ground $^4I_{15/2}$ state to the $^2H_{11/2}$ state more effectively. Finally, these excited Er^{3+} ions are eventually released from the first excited state ($^4I_{13/2}$) to the ground level ($^4I_{15/2}$) with the enhancement of light emission at 1540 nm.[16]

To investigate the annealing effect on enhancing the Er-related emission efficiency, different annealing temperatures were employed. Figure 6 shows the XRD spectra of the Er-doped ZnO NRAs grown on bare Si substrates, 20 and 30 nm thick Ag island films with different annealing temperatures, indicating that all diffraction peaks can be indexed to the wurtzite ZnO structure and there is no new phase, such as Er_2O_3, formed after annealing at 900 °C. However, we did notice that Er_2O_3 is formed after annealing at 950 °C, leading to low emission efficiency of Er^{3+} emission. The XPS measurements and their fitting curves of O_{1s} signal spectra of Er-doped ZnO NRAs on bare Si substrate with annealing temperature of 800, 850, and 900 °C are used to investigate the densities of oxygen defects as shown in Fig. 7. The peaks of the fitting curves for these three spectra are attributed to the bond of ZnO at 530.1 eV, the bond of oxygen vacancies at 530.8 eV, and the bond of OH^- at the surface of ZnO NRAs bond at 532 eV, respectively.[39,40] As the annealing temperature increases from 800 °C to 900 °C, the ratio of the intensity of oxygen vacancies at 530.8 eV to that of bond of

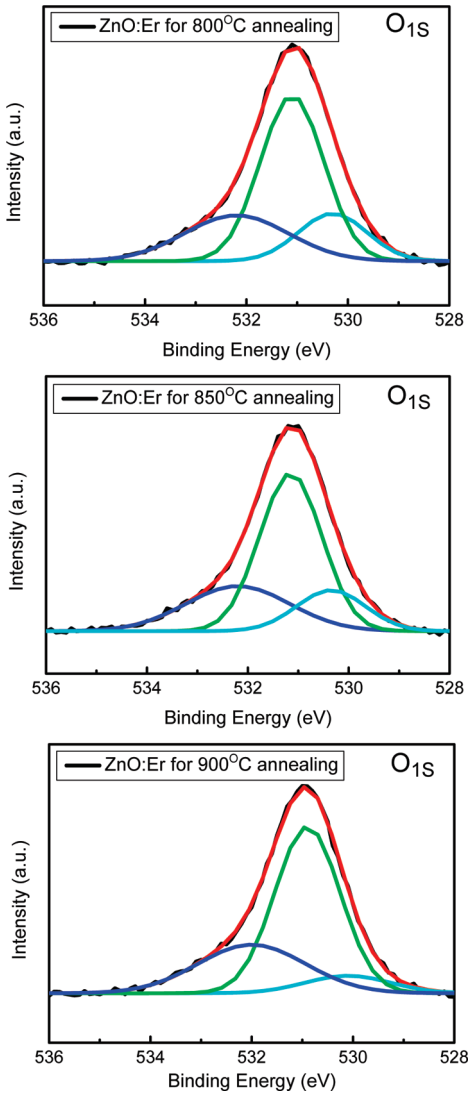

Figure 7. Fitting curves of O_{1S} signals of XPS for Er-doped ZnO NRAs grown on bare Si substrate with different annealing temperatures.

ZnO at 530.1 eV increases from 1.447 to 1.686. This suggests that the density of oxygen vacancies is increased with the annealing temperature. Moreover, a peak located at 529 eV related to Er_2O_3 is not observed, further supporting the XRD analysis that the Er atoms are incorporated into the wurtzite ZnO lattice rather than form the cubic Er_2O_3 crystal after the annealing of 900 °C for up to 4 h. However, a peak located at 529 eV can be found in the samples for 5 hour annealing at 900 °C, indicating the possible formation of cubic Er_2O_3 after a long-time high-temperature annealing process.

Figure 8a shows the PL intensity of the deep level emission at 540 nm for Er-doped ZnO NRAs on Si and Ag/Si substrates with the annealing temperatures of 800, 850, and 900 °C. The intensity of the deep level emission increases with the annealing temperatures for all samples. This phenomenon further supports the results of XPS that the density of the oxygen vacancies of Er-doped ZnO NRAs, which is responsible for the intensity of the deep level emission at 540 nm of ZnO host,[32] increases with the annealing temperatures. Accordingly, the deep level emission can be enhanced simultaneously by the increased density of deep level states via a high temperature annealing process together

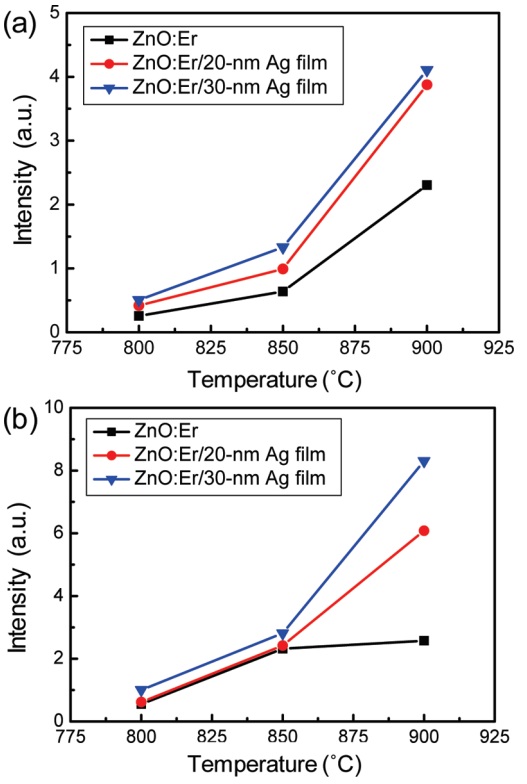

Figure 8. Annealing temperature-dependent PL intensities at (a) 540 and (b) 1540 nm of Er-doped ZnO NRAs on bare Si, 20 and 30 nm thick Ag island films/Si substrates.

with surface plasmon resonance coupled by the Ag island films. Figure 8b shows the PL intensity of the Er-related emission at 1540 nm for Er-doped ZnO NRAs on Si and Ag/Si substrates with different annealing temperatures. For the 1540 nm PL intensity (Figure 8b), a similar trend to the deep level emission (Figure 8a) is obtained, demonstrating the effective process of energy transfer from the deep level emission to Er^{3+} emission. Consequently, the enhancement of the 1540 nm emission from $^4I_{13/2}$ to $^4I_{15/2}$ in the Er-doped ZnO NRAs can be achieved by coupling the deep level emission improved by the Ag island films and the high temperature annealing.

CONCLUSION

In summary, the efficiency enhancement of 1540 nm emission from $^4I_{13/2}$ to $^4I_{15/2}$ in the single-crystal Er-doped ZnO NRAs was carried out by promoting deep level emission via the surface plasmon effect and the increase of the defect density. For coupling surface plasmon, 20-30 nm thick Ag island films were deposited before growing ZnO NRAs. As the size of Ag island films is increased, the intensity of the deep level emission at 540 nm is enhanced. The high annealing temperature ranging from 800 to 900 °C were used to increase the density of deep level states. On the basis of these results, Er-doped ZnO NRAs with Ag islands show a great promise as the material basis for developing ZnO-based light source in IR regions.

AUTHOR INFORMATION

Corresponding Author

*E-mail: jhhe@cc.ee.ntu.edu.tw.

REFERENCES

(1) Zavada, J. M.; Thaik, M.; Hommerich, U.; MacKenzie, J. D.; Abernathy, C. R.; Pearton, S. J.; Wilson, R. G. *J. Alloys Compd.* **2000**, *300*, 207–213.

(2) Zheng, B.; Michel, J.; Ren, F. Y. G.; Kimerling, L. C.; Jacobson, D. C.; Poate, J. M. *Appl. Phys. Lett.* **1994**, *64*, 2842–2844.

(3) Ishikawa, Y.; Okamoto, M.; Tanaka, S.; Nezaki, D.; Shibata, N. *J. Mater. Res.* **2005**, *20*, 2578–2582.

(4) Takahei, K.; Taguchi, A. *J. Appl. Phys.* **1993**, *74*, 1979–1982.

(5) Favennec, P. N.; Lharidon, H.; Salvi, M.; Moutonnet, D.; Leguillou, Y. *Electron. Lett.* **1989**, *25*, 718–719.

(6) Bresler, M. S.; Gusev, O. B.; Kudoyarova, V. K.; Kuznetsov, A. N.; Pak, P. E.; Terukov, E. I.; Yassievich, I. N.; Zakharchenya, B. P.; Fuhs, W.; Sturn, A. *Appl. Phys. Lett.* **1995**, *67*, 3599–3601.

(7) Steckl, A. J.; Devrajan, J.; Choyke, W. J.; Devaty, R. P.; Yoganathan, M.; Novak, S. W. *J. Electron. Mater.* **1996**, *25*, 869–873.

(8) Steckl, A. J.; Heikenfeld, J. C.; Lee, D. S.; Garter, M. J.; Baker, C. C.; Wang, Y. Q.; Jones, R. *IEEE J. Sel. Top. Quantum Electron.* **2002**, *8*, 749–766.

(9) Kong, J.; Zhu, H.; Li, R.; Luo, W.; Chen, X. *Opt. Express* **2009**, *34*, 1873–1875.

(10) Liu, Y.; Luo, W.; Li, R.; Zhu, H.; Chen, X. *Opt. Express* **2009**, *17*, 9748–9753.

(11) Fu, C.; Liao, J.; Luo, W.; Li, R.; Chen, X. *Opt. Lett.* **2008**, *33*, 953–955.

(12) Liu, Y.; Luo, W.; Li, R.; Liu, G.; Antonio, M. R.; Cheng, X. *J. Phys. Chem. C* **2008**, *112*, 686–694.

(13) Komuro, S.; Katsumata, T.; Morikawa, T.; Zhao, X.; Isshiki, H.; Aoyagi, Y. *Appl. Phys. Lett.* **2000**, *76*, 3935–3937.

(14) Sonder, E.; Zuhr, R. A.; Valiga, R. E. *J. Appl. Phys.* **1988**, *64*, 1140–1144.

(15) Wang, J.; Zhou, M. J.; Hark, S. K.; Li, Q.; Tang, D.; Chu, M. W.; Chen, C. H. *Appl. Phys. Lett.* **2006**, *89*, 221917.

(16) Yang, W. C.; Wang, C. W.; Wang, J. C.; Chang, Y. C.; Hsu, H. C.; Nee, T. E.; Chen, L. J.; He, J. H. *J. Nanosci. Nanotechnol.* **2008**, *8*, 3363–3368.

(17) Choi, H. J.; Shin, J. H.; Suh, K.; Seong, H. K.; Han, H. C.; Lee, J. C. *Nano Lett.* **2005**, *5*, 2432–2437.

(18) Hsin, C. L.; He, J. H.; Chen, L. *J. Appl. Phys. Lett.* **2006**, *88*, 063111.

(19) Chen, C. Y.; Chen, M. W.; Ke, J. J.; Lin, C. A.; Retamal, J. R. D.; He, J. H. *Pure Appl. Chem.* **2010**, *82*, 2055–2073.

(20) Egelhaaf, H. J.; Oelkrug, D. *J. Cryst. Growth* **1996**, *161*, 190–194.

(21) Lin, B. X.; Fu, Z. X.; Jia, Y. B. *Appl. Phys. Lett.* **2001**, *79*, 943–945.

(22) Gallis, S.; Huang, M. B.; Kaloyeros, A. E. *Appl. Phys. Lett.* **2007**, *90*, 161914.

(23) Fukushima, M.; Managaki, N.; Fujii, M.; Yanagi, H.; Hayashi, S. *J. Appl. Phys.* **2005**, *98*, 024316.

(24) Okamoto, K.; Niki, I.; Shvartser, A.; Narukawa, Y.; Mukai, T.; Scherer, A. *Nat. Mater.* **2004**, *3*, 601–605.

(25) Cheng, P. H.; Li, D. S.; Yuan, Z. Z.; Chen, P. L.; Yang, D. R. *Appl. Phys. Lett.* **2008**, *92*, 041119.

(26) Ong, H. C.; Lei, D. Y.; Li, J. *Proc. SPIE* **2007**, *6474*, 64740V1–64740V10.

(27) Chen, C. Y.; Lin, C. A.; Chen, M. J.; Lin, G. R.; He, J. H. *Nanotechnology* **2009**, *20*, 185605.

(28) Zhang, X. L.; Kang, Y. S. *Inorg. Chem.* **2006**, *45*, 4186–4190.

(29) Armelao, L.; Barreca, D.; Bottaro, G.; Gasparotto, A.; Leonarduzzi, D.; Maragno, C.; Tondello, E.; Sada, C. *J. Vac. Sci. Technol., A* **2006**, *24*, 1941–1947.

(30) Lang, W. C.; Padalia, B. D.; Watson, L. M.; Fabian, D. J.; Norris, P. R. *Faraday Discuss.* **1975**, *60*, 37–43.

(31) Ishii, M.; Komuro, S.; Morikawa, T.; Aoyagi, Y. *J. Appl. Phys.* **2001**, *89*, 3679–3684.

(32) Vanheusden, K.; Seager, C. H.; Warren, W. L.; Tallant, D. R.; Voigt, J. A. *Appl. Phys. Lett.* **1996**, *68*, 403–405.

(33) Zhao, Q. X.; Klason, P.; Willander, M.; Zhong, H. M.; Lu, W.; Yang, J. H. *Appl. Phys. Lett.* **2005**, *87*, 211912.

(34) Lakowicz, J. R. *Anal. Biochem.* **2005**, *337*, 171–194.

(35) Yeshchenko, O. A.; Dmitruk, I. M.; Alexeenko, A. A.; Losytskyy, M. Y.; Kotko, A. V.; Pinchuk, A. O. *Phys. Rev. B* **2009**, *79*, 235438.

(36) Jensen, T. R.; Duval, M. L.; Kelly, K. L.; Lazarides, A. A.; Schatz, G. C.; Van Duyne, R. P. *J. Phys. Chem. B* **1999**, *103*, 9846–9853.

(37) Jensen, T. R.; Malinsky, M. D.; Haynes, C. L.; Van Duyne, R. P. *J. Phys. Chem. B* **2000**, *104*, 10549–10556.

(38) Patole, S.; Islam, M.; Aiyer, R. C.; Mahamuni, S. *J. Mater. Sci.* **2006**, *41*, 5602–5607.

(39) Baek, S.; Song, J.; Lim, S. *Physica B* **2007**, *399*, 101–104.

(40) Song, J.; Baek, S.; Lim, S. *Physica B* **2008**, *403*, 1960–1963.